Юрій Володимирович Калюжний
Степан Петрович Глушак

Фазова рівновага полідисперсної багатоюкавівської рідини твердих сфер. Високотемпературне наближення

Роботу отримано 13 січня 2006 р.

Затверджено до друку Вченою радою ІФКС НАН України

Рекомендовано до друку семінаром відділу теорії розчинів

Виготовлено при ІФКС НАН України

Національна академія наук України

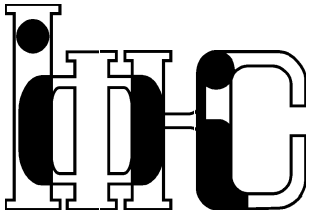

ІНСТИТУТ ФІЗИКИ КОНДЕНСОВАНИХ СИСТЕМ

ICMP–06–01E

Yu. V. Kalyuzhnyi, S. P. Hlushak

PHASE COEXISTENCE IN POLYDISPERSE MULTI-YUKAWA HARD-SPHERE FLUID. HIGH TEMPERATURE APPROXIMATION

ЛЬВІВ

УДК: 532; 532.74; 532.772

PACS: 05.70.Ce; 61.20.Gy; 82.70.Dd

Фазова рівновага полідисперсної багатоюкавівської рідини твердих сфер. Високотемпературне наближення

Ю. В. Калюжний, С. П. Глушак

Анотація. Фазові властивості полідисперсної багатоюкавівської суміші твердих сфер вивчалися в рамках високотемпературного наближення. Показано, що досліджувані моделі у високотемпературному наближенні належать до класу моделей із "заокругленою" вільною енергією, тобто моделей, термодинамічні властивості яких визначаються скінченною кількістю моментів. Використовуючи цю властивість, пораховано повну фазову діаграму та функції розподілу співіснуючих фаз для кількох моделей полідисперсних рідин. Зокрема, полідисперсну одноюкавівську суміш твердих сфер та рідину з взаємодією Леннарда-Джонса з полідисперсністю енергій взаємодії та розмірів, або тільки з полідисперсністю за розмірами.

Phase coexistence in polydisperse multi-Yukawa hard-sphere fluid. High temperature approximation

Yu. V. Kalyuzhnyi, S. P. Hlushak

Abstract. High temperature approximation (HTA) is used to describe the phase behavior of the polydisperse multi-Yukawa hard-sphere fluid mixture. It is demonstrated that in the frames of the HTA the model belongs to the class of "truncatable free energy models", i.e. the models with thermodynamical properties (Helmholtz free energy, chemical potential and pressure) defined by the finite number of generalized moments. Using this property we were able to calculate complete phase diagram (i.e., cloud and shadow curves as well as binodals) and distribution functions of the coexisting phases of several different models of polydisperse fluids. In particular, we consider polydisperse one-Yukawa hard-sphere mixture with factorizable Yukawa coefficients and polydisperse Lennard-Jones (LJ) mixture with interaction energy parameter and/or size polydispersity. To validate the accuracy of the HTA we compare theoretical results with previously published results of more advanced mean spherical approximation (MSA) for the one-Yukawa model and with Monte Carlo (MC) computer simulation results of Wilding et al. We find that overall predictions of the HTA are in reasonable agreement with predictions of the MSA and MC.

Подається в Журнал хімічної фізики
Submitted to Journal of Chemical Physics

1. Introduction

Understanding of the effects of polydispersity on the phase behavior, phase boundaries and fractionation of colloidal and polymeric fluids are of both fundamental and practical importance. Most of industrially important colloidal and polymeric materials are intrinsically polydisperse, i.e. each particle in the system is unique in size, charge, shape, chain length, etc. Usually in theoretical descriptions such systems are viewed as a mixture with infinite number of components, which offer very rich phase behavior with possibly new phases and new phase transitions. The main obstacle in theoretical studies of the phase behavior in polydisperse systems is due to the fact that now one have to deal with the infinite number of equations for coexisting phases. To deal with this problem several methods have been proposed [1,2] and used recently [1,3–5] to study phase behavior of the number of model polydisperse systems. However none of these studies goes in their sophistication beyond the van der Waals (vdW) [1,3] or the Onsager [5] level of description. In spite of the fact that a basic formalism for polydisperse systems has been developed already some time ago [6], only recently several studies, which account correlations on the level of the mean spherical approximation (MSA), have been published. These include polydisperse hard-sphere mixtures with one-Yukawa [7], Coulomb [8–10], and sticky [11] interactions outside the hard core. In the case of Yukawa and sticky potentials application of the MSA is restricted to the systems with factorized version of interaction, i.e. the matrix of the coefficients describing the strength of the corresponding interaction is factorized into the product of two vectors. The models, studied in these publications in the frames of the MSA belong to the family of so-called 'truncatable' free energy models [2]. These are the models with Helmholtz free energy being completely defined by a finite number of generalized moments of the corresponding distribution function. This feature allows one to map the infinite set of equations for the phase equilibria onto a finite set of equations for the moments.

In this paper we propose hight temperature approximation (HTA) for polydisperse multi-Yukawa hard-sphere fluid. We demonstrate that within HTA this system belongs to the family of truncatable free energy models. Unlike MSA HTA includes correlations on the level of the hard-sphere system, however it is not restricted to the case of factorized one-Yukawa potential only. The latter feature gives us more flexibility in choosing the systems to be studied. To verify the accuracy of the theory we calculate the full phase diagram (including binodals, cloud and shadow curves, distribution functions of the coexisting phases) for poly-

disperse one-Yukawa hard-sphere fluid and polydisperse Lennard-Jones fluid and compare our results with corresponding results of the MSA [7] and Monte Carlo (MC) method [4,12]. The paper is organized as follows:

2. Phase equilibrium conditions

In dealing with polydisperse fluids it is convenient to start with the version of the system with arbitrary but finite number of components and on the final step switch all the expressions to polydisperse case.

2.1. Multicomponent case

We consider p-component system with q coexisting phases. Each phase consists of $N_i^{(\alpha)}$ particles of species i and occupies the volume $V^{(\alpha)}$, where the upper index α denote the phase. It is assumed that the total number of the particles $N_i^{(0)}$ of species i and total volume $V^{(0)}$ of the system are held constant, i.e.

$$V^{(0)} = \sum_{\alpha=1}^{q} V^{(\alpha)} \tag{1}$$

$$N_i^{(0)} = \sum_{\alpha=1}^{q} N_i^{(\alpha)}, \quad i = 1, \ldots, p. \tag{2}$$

Hereafter the value of the upper index $\alpha = 0$ denotes the properties of the parent phase, which under certain conditions can be separated into q coexisting phases. Helmholtz free energy A of such system is

$$A = \sum_{\alpha=1}^{q} A^{(\alpha)} \left(T, V^{(\alpha)}, \left\{ N_i^{(\alpha)} \right\} \right) \tag{3}$$

where $A^{(\alpha)}(\ldots)$ is Helmholtz free energy of the phase α and $\left\{ N_i^{(\alpha)} \right\}$ denotes the set $N_1^{(\alpha)}, N_2^{(\alpha)}, ..., N_p^{(\alpha)}$. At equilibrium the free energy (3) has its minimum value provided that conditions (1) and (2) are satisfied. Using Lagrange multiplier method we recover well known phase equilibrium conditions for multicomponent system

$$\mu_i^{(1)} \left(T, V^{(1)}, \left\{ N_i^{(1)} \right\} \right) = \ldots = \mu_i^{(q)} \left(T, V^{(q)}, \left\{ N_i^{(q)} \right\} \right), \quad i = 1, \ldots, p, \tag{4}$$

and

$$P^{(1)} \left(T, V^{(1)}, \left\{ N_i^{(1)} \right\} \right) = \ldots = P^{(q)} \left(T, V^{(q)}, \left\{ N_i^{(q)} \right\} \right). \tag{5}$$

where $\mu_i^{(\alpha)}$ is the chemical potential of the particles of species i in the phase α and $P^{(\alpha)}$ is the pressure of the phase α. Solution of this set of $(p+1)(q-1)$ equations together with the set of $p+1$ additional conditions (1) and (2) will give us $(p+1)q$ unknowns $N_i^{(\alpha)}, V^{(\alpha)}, \quad i = 1, \ldots, p, \quad \alpha = 1, \ldots, q,$. Note, that each phase will differ not only by its volume, but also by its distribution of the particles of different species.

2.2. Polydisperse case

To extend the phase equilibrium conditions (5) and (5) to the case of polydisperse system it is more convenient to use instead of the set of variables $V^{(\alpha)}$ and $N_i^{(\alpha)}$ the set, which includes the density of the phase α, $\rho^{(\alpha)} = N^{(\alpha)}/V^{(\alpha)}$, and two types of the fractions, i.e.

$$x_i^{(\alpha)} = N_i^{(\alpha)}/N^{(\alpha)} \tag{6}$$

$$x^{(\alpha)} = N^{(\alpha)}/N^{(0)}, \tag{7}$$

where

$$N^{(\alpha)} = \sum_{i=1}^{n} N_i^{(\alpha)}. \tag{8}$$

Now the set of equilibrium conditions (5) and (5) together with additional constrains (1) and (2) can be recast in the following form

$$\mu_i^{(1)} \left(T, \rho^{(1)}, \left\{ x_i^{(1)} \right\} \right) = \ldots = \mu_i^{(q)} \left(T, \rho^{(q)}, \left\{ x_i^{(q)} \right\} \right), \tag{9}$$

$$P^{(1)} \left(T, \rho^{(1)}, \left\{ x_i^{(1)} \right\} \right) = \ldots = P^{(q)} \left(T, \rho^{(q)}, \left\{ x_i^{(q)} \right\} \right), \tag{10}$$

$$v^{(0)} = \sum_{\alpha=1}^{q} v^{(\alpha)} x^{(\alpha)}, \tag{11}$$

$$x_i^{(0)} = \sum_{\alpha=1}^{q} x_i^{(\alpha)} x^{(\alpha)}, \tag{12}$$

with the fractions $x_i^{(\alpha)}$ satisfying the following normalizing condition

$$\sum_{i=1}^{n} x_i^{(\alpha)} = 1, \tag{13}$$

where $v^{(0)} = 1/\rho^{(0)}$ and $v^{(\alpha)} = 1/\rho^{(\alpha)}$.

Now extension of the phase equilibrium conditions to the case of polydisperse system is straightforward and can be achieved by switching from discrete species index i to its continuous counterpart ξ via the following substitution rule [18]

$$x_i \to F(\xi)\, d\xi, \tag{14}$$

with $F(\xi)$ being a positive distribution function normalized to 1. It should be pointed out that ξ can be multidimensional. Due to this substitution, summations over i in (9)-(13) become integrations over ξ and thermodynamic properties become *functionals* of the distribution function $F(\xi)$, which we will indicate by the square brackets. We have

$$\mu^{(1)}\left(\xi, T, \rho^{(1)}, \left[F^{(1)}(\xi)\right]\right) = \ldots = \mu^{(q)}\left(\xi, T, \rho^{(q)}, \left[F^{(q)}(\xi)\right]\right) \tag{15}$$

$$P^{(1)}\left(T, \rho^{(1)}, \left[F^{(1)}(\xi)\right]\right) = \ldots = P^{(q)}\left(T, \rho^{(q)}, \left[F^{(q)}(\xi)\right]\right). \tag{16}$$

$$v^{(0)} = \sum_{\alpha=1}^{q} v^{(\alpha)} x^{(\alpha)}, \tag{17}$$

$$F^{(0)}(\xi) = \sum_{\alpha=1}^{q} F^{(\alpha)}(\xi)\, x^{(\alpha)}, \tag{18}$$

$$\int F^{(\alpha)}(\xi)\, d\xi = 1. \tag{19}$$

Formally the set of relations (15)-(19) form a closed set of equations for the unknowns $\rho^{(\alpha)}$, $x^{(\alpha)}$ and $F^{(\alpha)}(\xi)$, which can be solved as soon as expressions for the thermodynamical properties of the corresponding polydisperse system at hand will be available.

At present this problem seems to be solvable only for the so-called truncatable free energy models, i.e. these models, for which thermodynamic properties can be represented by a finite number of (generalized) moments of the distribution function $F(\xi)$.

2.3. Two-phase equilibrium conditions for the free energy truncatable models

In this section we will consider two-phase equilibrium conditions specialized to the case of truncatable free energy models. In our consideration we will follow the general scheme developed by Bellier-Castella et al. [1]. We assume that thermodynamical properties of the model depends on $K+1$ generalized moments $m_0, m_1, ..., m_K$, which are defined as follows

$$m_k = \rho \int d\xi\; m_k(\xi), \qquad k \neq 0 \tag{20}$$

and $m_0 = \rho$.

Now the set of the conditions (15)- (19) takes the following form

$$\mu^{(1)}\left(\xi, T, \left\{m_k^{(1)}\right\}\right) = \mu^{(2)}\left(\xi, T, \left\{m_k^{(2)}\right\}\right), \tag{21}$$

$$P^{(1)}\left(T, \left\{m_k^{(1)}\right\}\right) = P^{(2)}\left(T, \left\{m_k^{(2)}\right\}\right). \tag{22}$$

$$\rho^{(2)} F^{(2)}(\xi) = \frac{\rho^{(1)} - \rho^{(2)}}{\rho^{(1)} - \rho^{(0)}} \rho^{(0)} F^{(0)}(\xi) + \frac{\rho^{(2)} - \rho^{(0)}}{\rho^{(1)} - \rho^{(0)}} \rho^{(1)} F^{(1)}(\xi), \tag{23}$$

$$\int F^{(\alpha)}(\xi)\, d\xi = 1. \tag{24}$$

where $\left\{m_k^{(\alpha)}\right\}$ denotes the set $m_0^{(\alpha)}, m_1^{(\alpha)}, ..., m_K^{(\alpha)}$.

Condition on the equality of the chemical potentials in two phases (21) can be written in terms of the excess values of the chemical potentials $\mu_{ex}^{(\alpha)}$

$$\ln\left(\frac{F^{(1)}(\xi)\,\rho^{(1)}}{F^{(2)}(\xi)\,\rho^{(2)}}\right) = \Delta\mu_{ex}\left(\xi, T, \left\{m^{(1)}\right\}, \left\{m^{(2)}\right\}\right), \tag{25}$$

where

$$\Delta\mu_{ex}\left(\xi, T, \left\{m^{(1)}\right\}, \left\{m^{(2)}\right\}\right) = \mu_{ex}^{(2)}\left(\xi, T, \left\{m^{(2)}\right\}\right) - \mu_{ex}^{(1)}\left(\xi, T, \left\{m^{(1)}\right\}\right). \tag{26}$$

This allows us to relate distribution functions $F^{(\alpha)}(\xi)$ in the two different phases

$$F^{(1)}(\xi) = F^{(2)}(\xi)\, A_{12}\left(\xi, T, \left\{m^{(1)}\right\}\left\{m^{(2)}\right\}\right), \tag{27}$$

where

$$A_{12}\left(\xi,T,\left\{m^{(1)}\right\}\left\{m^{(2)}\right\}\right) = \frac{\rho^{(2)}}{\rho^{(1)}}\exp\left[\Delta\mu_{ex}\left(\xi,T,\left\{m^{(1)}\right\}\left\{m^{(2)}\right\}\right)\right], \quad (28)$$

Taking into account (23), (27) and definition (20) we get

$$F^{(1)}(\xi) = F^{(0)}(\xi)\,H\left(\xi,T,m_0^{(2)},\left\{m^{(1)}\right\}\left\{m^{(0)}\right\}\right), \quad (29)$$

$$m_k^{(2)} = \frac{\rho^{(1)}-\rho^{(2)}}{\rho^{(1)}-\rho^{(0)}}m_k^{(0)} + \frac{\rho^{(2)}-\rho^{(0)}}{\rho^{(1)}-\rho^{(0)}}m_k^{(1)}, \quad (30)$$

where

$$H\left(\xi,T,m_0^{(2)},\left\{m^{(1)}\right\}\left\{m^{(0)}\right\}\right) = \frac{\left(\rho^{(1)}-\rho^{(2)}\right)A_{12}\left(\xi,T,m_0^{(2)},\left\{m^{(1)}\right\}\left\{m^{(0)}\right\}\right)}{\left(\frac{\rho^{(2)}\rho^{(1)}}{\rho^{(0)}}-\rho^{(2)}\right)+\left(\rho^{(1)}-\frac{\rho^{(2)}\rho^{(1)}}{\rho^{(0)}}\right)A_{12}\left(\xi,T,m_0^{(2)},\{m^{(1)}\}\{m^{(0)}\}\right)}. \quad (31)$$

Note that H and A_{12} depend on the all moments of the phases 0 and 1 and only on the zero moment (density) of the phase 2, since all the rest of the moments of the second phase are connected to the moments of the phases 0 and 1 via relation (30)

Now the set of equations (21) and (22) can be solved in terms of the moments of coexisting phases. The corresponding set of equations follows from the definition (20)

$$m_k^{(1)} = m_0^{(1)}\int d\xi m_k^{(1)}(\xi)\,F^{(0)}(\xi)\,H\left(\xi,T,m_0^{(2)},\left\{m^{(1)}\right\}\left\{m^{(0)}\right\}\right) \quad (32)$$

where $k=1,2,...,K$. Equation (32) together with the equation for the equality of the pressure in both phases

$$P^{(1)}\left(\xi,T,\left\{m^{(1)}\right\}\left\{m^{(0)}\right\}\right) = P^{(2)}\left(\xi,T,m_0^{(2)},\left\{m^{(1)}\right\}\left\{m^{(0)}\right\}\right) \quad (33)$$

and normalizing condition (24) for either $\alpha=1$ or $\alpha=2$ form a closed set of equations for $K+2$ unknowns $\left\{m^{(1)}\right\}, m_0^{(2)}$. Thus solution of the set of equations (24), (32), (33) for a given temperature T, density of the parent phase $\rho^{(0)}$, and parent distribution function $F^{(0)}(\xi)$ gives the coexisting densities $\rho^{(\alpha)}$ of the two daughter phases and corresponding distribution functions $F^{(\alpha)}(\xi)$, $\alpha=1,2$. The coexistence densities for different temperatures fix binodals, which are terminated at a temperature for which

the density of one of the phases is equal to the density $\rho^{(0)}$ of the parent phase; these termination points form the so-called cloud and shadow curves which thus represent an envelope for the binodals. Cloud and shadow curves intersect at the critical point, which is characterized by the critical temperature $T_{\rm cr}$ and critical density $\rho_{\rm cr}=\rho^{(1)}=\rho^{(2)}=\rho^{(0)}$. Thus only for $\rho^{(0)}=\rho_{\rm cr}$ the two branches of the binodal meet at the critical point.

By definition, states located on the cloud curve are characterized that they coexist with a state (localized on the shadow curve) where an infinitely small amount of the other phase emerges. Thus the cloud and shadow curves can be obtained as special solutions of the general phase coexistence problem, when the properties of one phase are equal to the properties of the parent phase: assuming, e.g., the second phase to be the cloud phase, i.e. $\rho^{(2)}=\rho^{(0)}$, and following the scheme presented above we will end up with the same set of equations, (24), (32), (33), but with $\rho^{(2)}$ and $F^{(2)}(\xi)$ substituted by $\rho^{(0)}$ and $F^{(0)}(\xi)$, respectively. Note that $F^{(2)}(\xi)=F^{(0)}(\xi)$ is now known, but $\rho^{(0)}$ is unknown; it is obtained from the solution of the appropriately modified set of equations (24), (32), (33).

3. Thermodynamical properties of the multi-Yukawa hard-sphere fluid

We consider the fluid with interparticle pair potential represented by the multi-Yukawa hard-sphere potential

$$V_{ij}(r) = \begin{cases} \infty, & \text{for } r\le\sigma_{ij},\\ -\frac{\epsilon_0}{r}\sum_n^{N_Y}\sum_m^{M}\frac{(-1)^{m-1}}{z_n}A_i^{(nm)}A_j^{(nm)}e^{-z_n(r-\sigma_{ij})} & \\ & \text{for } r>\sigma_{ij}, \end{cases} \quad (34)$$

where $\sigma_{ij}=(\sigma_i+\sigma_j)/2$ and σ_i is the hard-sphere diameter of the particle of species i.

The form suggested for the potential (34) is very flexible and can be used to model a large variety of the realistic potentials by appropriate choice for the coefficients A_i^{nm} and z_n [16,17].

3.1. High temperature approximation

The high temperature approximation (HTA), applied in this study, will be obtained using Gibbs-Bogoliubov inequality [19]

$$A - A_0 \le \langle (H-H_0)\rangle_0 . \quad (35)$$

where A_0 is the Helmholtz free energy of the reference system.

Choosing the hard-sphere system to be a reference system and using the upper limit of this inequality we recover HTA

$$\frac{\beta A}{V} = \frac{\beta A_{HS}}{V} + 2\pi\beta \sum_i \sum_j \rho_i \rho_j \int_0^\infty dr r^2 V_{ij}(r)\, g_{ij}^{HS}(r). \tag{36}$$

where $g_{ij}^{HS}(r)$ is the hard-sphere radial distribution function. Substituting into (36) expression for the pair potential (34) we have

$$\frac{\beta A}{V} = \frac{\beta A_{HS}}{V} - 2\pi\beta\epsilon_0 \sum_i \sum_j \rho_i \rho_j \sum_n^{N_Y} \sum_m^M \frac{(-1)^{m-1}}{z_n} A_i^{(nm)} A_j^{(nm)} \tilde{G}_{ij}^{HS}(z_n). \tag{37}$$

where $\tilde{G}_{ij}^{HS}(z_n)$ is the Laplace transform of hard-sphere radial distribution function

$$\tilde{G}_{ij}^{(HS)}(z_n) = e^{z_n \sigma_{ij}} \int_0^\infty dr r e^{-z_n r} g_{ij}^{(HS)}(r). \tag{38}$$

We will be using here Percus-Yewick approximation for hard-sphere radial distribution function, since analytical expression for its Laplace transform is known [20,21]

$$\tilde{G}_{ij}^{(HS)}(z_n) =!!!![1] = \frac{\Delta}{z_n^2 \tilde{D}_0^{(n)}} \left\{ z_n \left[\sigma_{ij} + \sigma_i \sigma_j \frac{\pi}{4\Delta} m_2 \right] + 1 + \frac{\pi}{2\Delta} m_3 + \frac{\pi z_n}{2\Delta} \left(m_2^{(n)} - 2\sigma_{ij} m_1^{(n)} + \sigma_i \sigma_j m_0^{(n)} \right) \right\}, \tag{39}$$

where

$$\tilde{D}_0^{(n)} = \Delta^2 - \frac{2\pi}{z_n} \left(1 + \frac{1}{2}\pi m_3 \right) \left(m_0^{(n)} + \frac{1}{2} m_2 \right) - 2\pi \left\{ \Delta m_1^{(n)} + \frac{1}{4}\pi \left[m_2^{(n)} \left(m_2 + 2m_0^{(n)} \right) - \left(m_1^{(n)} \right)^2 \right] \right\}, \tag{40}$$

$$m_l = \sum_k \rho_k m_l(k); \quad m_l(k) = \sigma_k^l, \tag{41}$$

$$m_l^{(n)} = \sum_k \rho_k m_l^{(n)}(k); \quad m_l^{(n)}(k) = \sigma_k^l \varphi(z_n, \sigma_k), \tag{42}$$

$$\Delta = 1 - \pi m_3/6, \tag{43}$$

$$\varphi(z_n, \sigma) = \frac{1}{z_n^2} \left(1 - z_n \sigma - e^{-z_n \sigma} \right) \tag{44}$$

To extend the expressions for thermodynamical properties for polydisperse case it is convenient to represent expression for Helmholtz free energy (38) in terms of the moments. Introducing in addition to already existing moments m_l and $m_l^{(n)}$ one more

$$m_l^{(nm)} = \sum_k \rho_k m_l^{(nm)}(k); \quad m_l^{(nm)}(k) = \sigma_k^l A_k^{(nm)}, \tag{45}$$

we have

$$\frac{\beta A}{V} = \frac{\beta A_{HS}}{V} - 2\pi\beta\epsilon_0 \sum_n^{N_Y} \sum_m^M \frac{(-1)^{m-1} Q_0^{(nm)}}{z_n^3 \tilde{D}_0^{(n)}} \tag{46}$$

where

$$Q_0^{(nm)} = \left[\Delta + \pi \left(m_3 + \frac{1}{2} z_n m_2^{(n)} \right) \right] \left[\left(m_0^{(nm)} \right)^2 + \left(m_1^{(nm)} \right)^2 \right] + z_n \left(\Delta - \pi m_1^{(n)} \right) m_0^{(nm)} m_1^{(nm)}. \tag{47}$$

Differentiating expression for Helmholtz free energy (46) with respect to the density we will have the following expression for the chemical potential

$$\beta\mu_k = \frac{\partial}{\partial\rho_k} \left(\frac{\beta A}{V} \right) = \beta\mu_k^{(HS)} - 2\pi\beta\epsilon_0 \sum_n^{N_Y} \sum_m^M \frac{(-1)^{m-1}}{z_n^3 \tilde{D}_0^{(n)}} \left(\frac{\partial Q_0^{(nm)}}{\partial\rho_k} - \frac{Q_0^{(nm)}}{z_n^2 \tilde{D}_0^{(n)}} \frac{\partial \tilde{D}_0^{(n)}}{\partial\rho_k} \right), \tag{48}$$

where

$$\frac{\partial Q_0^{(nm)}}{\partial\rho_k} = \frac{1}{2}\pi \left(\frac{5}{3} m_3(k) + z_n m_2^{(n)}(k) \right) \left[\left(m_0^{(nm)} \right)^2 + \left(m_1^{(nm)} \right)^2 \right] + 2 \left[m_0^{(nm)} m_0^{(nm)}(k) + m_1^{(nm)} m_1^{(nm)}(k) \right] \left[\Delta + \pi \left(m_3 + \frac{1}{2} z_n m_2^{(n)} \right) \right] - \pi z_n \left(\frac{1}{6} m_3(k) + m_1^{(n)}(k) \right) m_0^{(nm)} m_1^{(nm)} + z_n \left(\Delta - \pi m_1^{(n)} \right) \left[m_1^{(nm)} m_0^{(nm)}(k) + m_0^{(nm)} m_1^{(nm)}(k) \right], \tag{49}$$

$$\frac{1}{2\pi}\frac{\partial\tilde{D}_0^{(n)}}{\partial\rho_k} = \frac{1}{3}\pi m_3(k)\left[\frac{1}{2}m_1^{(n)} - \frac{1}{z_n}\left(m_0^{(n)} + \frac{1}{2}m_2\right)\right] - \Delta\left(\frac{1}{6}m_3(k) + m_1^{(n)}(k)\right) - \left(\frac{1}{2}m_2(k) + m_0^{(n)}(k)\right)\left[\frac{1}{z_n}\left(\Delta + \frac{1}{2}\pi m_3\right) + \frac{1}{2}\pi m_2^{(n)}\right] - \frac{1}{4}\pi m_2^{(n)}(k)\left(m_2 + 2m_0^{(n)}\right) - 2m_1^{(n)}m_1^{(n)}(k). \quad (50)$$

The pressure P of the system can be calculated invoking the following general relation

$$\beta P = \beta\sum_k \rho_k\mu_k - \frac{\beta A}{V} \quad (51)$$

Here $\mu_{HS,k}$ and P_{HS} are the hard-sphere chemical potential and pressure, which in this study is represented by the Mansoori-Carnahan-Starling-Leland approximation [22]

$$\mu_{HS,k} = \mu_{id,k} + \mu_{HS,k}^{ex}, \quad (52)$$

where

$$\beta\mu_{HS,k}^{ex} = \frac{\beta A_{cs}^{ex}}{N} + \left(\frac{m_2}{m_3}\right)^2\left[3\sigma_k^2 - \frac{m_2}{m_0m_3}\left(m_3 + 2m_0\sigma_k^3\right)\right]\ln\Delta - \frac{\pi\sigma_k}{2\Delta}\left[\frac{1}{3}\left(\frac{m_2^3}{m_0m_3^2} - 1\right)\sigma_k^2m_0 - m_2 - \sigma_km_1\right] - \frac{\pi m_2}{2m_0\Delta^2}\left[m_1\left(\Delta - \frac{\pi}{6}\sigma_k^3\right) - \frac{\sigma_k^2m_2}{m_3}\right] + \frac{\pi m_2^3}{6m_3^2m_0\Delta}\left[\Delta\left(\sigma_k^3m_0 + m_3\right) - \frac{\pi}{3}m_3m_0\sigma_k^3\right] \quad (53)$$

and

$$\frac{\beta A_{cs}^{ex}}{N} = \left(\frac{m_2^3}{m_0m_3^2} - 1\right)\ln\Delta + \frac{\pi}{2\Delta}\frac{m_2}{m_0}\left(m_1 + \frac{1}{3}\frac{m_2^2}{m_3\Delta}\right). \quad (54)$$

$$\beta P_{HS} = \frac{1}{\Delta}\left[m_0 + \frac{\pi}{2\Delta}m_1m_2 + \frac{\pi^2}{12\Delta^2}m_2^3 - \frac{\pi^3}{216\Delta^2}m_2^3m_3\right] \quad (55)$$

Expressions for thermodynamical properties (46)-(55) are written in terms of the moments (41)-(45) and their extension to the polydisperse

case is straightforward. This goal can be achieved by substituting all the sums with respect to the discrete species index k by integration with respect to the multidimensional species index $\xi = (\sigma, \{A^{nm}\})$. Here $\left\{A^{(nm)}\right\}$ represent the set of all coefficients of the Yukawa potential (34). Now for the moments (41)-(45) and for the pressure expression (57) we have

$$m_l = \rho\int d\xi\; m_l(\xi)F(\xi),$$
$$m_l^{(n)} = \rho\int d\xi\; m_l^{(n)}(\xi)F(\xi),$$
$$m_l^{(nm)} = \rho\int d\xi\; m_l^{(nm)}(\xi)F(\xi) \quad (56)$$

and

$$P = \rho\int d\xi\;\mu(\xi)F(\xi) - \frac{A}{V}, \quad (57)$$

where

$$m_l(\xi) = \sigma^l$$
$$m_l^{(n)}(\xi) = \sigma^l\varphi_1(z_n,\sigma)$$
$$m_l^{(nm)}(\xi) = \sigma^lA^{(nm)} \quad (58)$$

One can see, that our multi-Yukawa hard-sphere system treated in the HTA belongs to the class of truncatable free energy models with thermodynamic properties defined by $2MN_Y + 3N_Y + 4$ generalized moments. Thus the formalism developed in the previous section can be used to predict the phase diagrams of the polydisperse version of the model.

4. Results and discussion

To illustrate the theory developed above and to verify its accuracy we consider two versions of polydisperse fluid. The first one is represented by polydisperse one-Yukawa hard-sphere mixture with factorizable Yukawa potential and the second one by polydisperse mixture of Lennard-Jones (LJ) particles. Both system were studied resently using mean spherical approximation (MSA) in the case of one-Yukawa model [15] and using Monte-Carlo simulation method in the case of LJ model [4,12].

4.1. One-Yukawa hard-sphere model

In the one-Yukawa case all the coefficients $A_i^{(nm)}$ are equal zero, except $A_i^{(11)}$, i.e. $A_i^{(11)} = Z_i/\sqrt{z_n\sigma_0}$. We will be using here HTA approximation and compare their results with results of more advanced MSA.

For the sake of simplicity we have chosen the distribution $F(\sigma, Z)$, which strongly correlate the size σ and the 'charge' parameter Z of the particles

$$F(\sigma, Z) = f(\sigma)\delta\left(Z - Z_0\frac{\sigma^2}{\langle\sigma^2\rangle}\right). \tag{59}$$

This choice states that the charge is proportional to the surface of the particles. For $f(\sigma)$ we have chosen the Beta-distribution, given by

$$f(\sigma) = \sigma_m^{-1}B^{-1}(\alpha,\beta)\left(\frac{\sigma}{\sigma_m}\right)^{\alpha-1}\left(1-\frac{\sigma}{\sigma_m}\right)^{\beta-1}\Theta(\sigma_m-\sigma)\Theta(\sigma) \tag{60}$$

Here $B(\alpha,\beta)$ is the beta function [23], α and β are related to the first ($\sigma_0 = \langle\sigma\rangle$) and the second ($\langle\sigma^2\rangle$) moments of $f(\sigma)$ by

$$\alpha = \frac{\sigma_m - \sigma_0\,(1+D_\sigma)}{\sigma_m D_\sigma}; \qquad \beta = \left(\frac{\sigma_m-\sigma_0}{\sigma_0}\right)\alpha \tag{61}$$

with $D_\sigma = \langle\sigma^2\rangle/\sigma_0^2 - 1$.

We present results for the phase diagram of a system, which is characterized by a parent distribution function $f_0(\sigma)$ represented by the Beta-distribution (60) with $D_\sigma = 0.02$ and $\sigma_m = 2\sigma_0$. The screening length of the Yukawa potential was chosen to be $z\sigma_0 = 1.8$. In what follows the temperature T and density ρ of the system will be represented by the dimensionless quantities $T^* = kT/(\epsilon_0 Z_0^2)$ and $\rho^* = \rho\sigma_0^3$, respectively.

In Figure 1 we show the phase diagram of the one-Yukawa system in the (T^*, ρ^*)-plane obtained using MSA and HTA theories, which includes cloud- and shadow-curves, and critical binodals. For the critical point MSA gives $T^*_{\rm cr,MSA} = 1.343$ and $\rho^*_{\rm cr,MSA} = 0.356$. Parameters of the critical point, which follow from the HTA are $T^*_{\rm cr,HTA} = 1.405$ and $\rho^*_{\rm cr,HTA} = 0.388$. For the reference we have added the phase coexistence curve for a one component system, treated as well in the MSA and HTA, characterized by a diameter $\sigma_{\rm oc} = \sigma_0$ and a 'charge' parameter $Z_{\rm oc} = Z_0$.

Both theories provide with quantitatively close predictions for the phase behavior of the model. Polydispersity do not change much the relation between MSA and HTA phase diagrams, i.e. in both monodisperse and polydisperse cases HTA shifts the MSA critical temperature towards $\approx 4.5\%$ higher values and MSA critical density towards $\approx 4\%$ lower values. Information about the composition of the coexisting phases and fractionation effects can be extracted from the distribution functions of the two daughter phases. For the two selected pairs of points on the phase coexistence curves (C_1, C_2 and E_1, E_2) at $T^* = 0.9$ (Figure 1) the daughter distribution functions, $f_1(\sigma)$ and $f_2(\sigma)$, together with the parent distribution function, $f_0(\sigma)$, are shown in Figures 2 and 3, respectively. For the points C_1 and C_2, which are located on the critical binodal ($\rho^{*(0)} = \rho^*_{\rm cr}$) the gas phase on average has smaller size particles, than the liquid phase. Points E_1 and E_2 are located on the cloud- and on the shadow-curve: by definition $f_1(\sigma) = f_0(\sigma)$ and one can see a substantial shift of the maximum of $f_2(\sigma)$ towards larger particles. In both cases results of the HTA and MSA almost coincide. In Figures 4 and 5 we show the evolution of the mean size of the particles $\langle\sigma\rangle_i$ and degree of polydispersity $D_{\sigma;i}$

$$\langle\sigma^n\rangle_i = \int_0^\infty d\sigma f_i(\sigma)\sigma^n, \qquad D_{\sigma;i} = \frac{\langle\sigma^2\rangle_i}{\sigma_0^2} - 1, \tag{62}$$

along the shadow curve. Here $n = 1, 2;\ n = 1, 2$. Both theories predict the same qualitative behavior with a certain quantitative difference due to the difference in predicting the critical temperature. With the temperature decrease one can see a strong increase in the mean size of the fluid phase particles and a slight decrease in the mean size of the gas phase particles (Figure 4). The width of both daughter distribution functions is smaller than that of the parent distribution function. One can see a strong decrease of the width of the liquid phase distribution function due to the temperature decrease. At the same time the width of the gas phase distribution function remains close to that of the parent phase.

4.2. LJ model

We will follow the previous studies [4,12] and consider polydisperse mixture of the LJ particles with the following pair potential

$$V_{LJ}(r;\sigma_1,\sigma_2) = 4\epsilon(\sigma_1,\sigma_2)\left[\left(\frac{\sigma_{12}}{r}\right)^{12} - \left(\frac{\sigma_{12}}{r}\right)^{6}\right], \tag{63}$$

where $\sigma_{12} = (\sigma_1+\sigma_2)/2$ and in the computer simulation studies this potential was terminated at $r > r^{(c)}(\sigma_1,\sigma_2) = 2.5\sigma_{12}$. LJ diameter σ was chosen to be distributed according to the gamma (Schultz) distribution

[24]

$$f(\sigma) = \left(\frac{\gamma+1}{\sigma_0}\right)^{\gamma+1} \frac{\sigma^\gamma}{\Gamma(\gamma+1)} \exp\left[-\frac{\gamma+1}{\sigma_0}\sigma\right], \qquad (64)$$

where σ_0 is the average particle diameter, $\Gamma(z)$ is the gamma function and γ is related to the distribution function width D_σ, i.e. $\gamma = 1/D_\sigma - 1$.

Two versions of polydisperse LJ mixture have been studied earlier by the MC simulation method. In the first version the LJ energy parameter was assumed to be independent of the sizes of the particles [4], i.e. $\epsilon(\sigma_1, \sigma_2) = \epsilon_0$. In the second version [12] $\epsilon(\sigma_1, \sigma_2)$ was chosen to have the following functional dependence: $\epsilon(\sigma_1, \sigma_2) = \sigma_1\sigma_2$. In both cases LJ potential (63) was substituted by the multi-Yukawa potential (34) with the hard-sphere sizes equal to the LJ particles sizes. Yukawa coefficients, which in polydisperse case become a functions of σ, i.e. $A_i^{(nm)} \to A^{(nm)}(\sigma)$, were calculated via the fitting procedure, described in the Appendix A.

To account for the truncation of the LJ potential Yukawa potential (34) was terminated at $r_{ij}^{(c)} = 3\sigma_{ij}$. The key integral of the HTA approach (36) was calculated using the following approximation

$$\int_0^\infty dr r^2 \theta(r_{ij}^{(c)} - r) V_{ij}(r)\, g_{ij}^{HS}(r) = \\ = \int_0^\infty dr r^2 V_{ij}(r)\, g_{ij}^{HS}(r) - \int_{r_{ij}^{(c)}}^\infty dr r^2 V_{ij}(r). \qquad (65)$$

where $\theta(\ldots)$ is the Heaviside step function.

As a result additional terms, which contain $3MN_Y$ new generalized moments, appear in the expressions for the chemical potential (48) and pressure (51). The final expressions for the chemical potential $\mu^{(tr)}$ and pressure $P^{(tr)}$ of the system with truncated Yukawa potential are

$$\beta\mu_k^{(tr)} = \beta\mu_k + \beta\Delta\mu_k^{(tr)}, \qquad P^{(tr)} = P + \Delta P^{(tr)}, \qquad (66)$$

where μ_k and P follows from expressions (48) and (51), respectively, and expressions for $\Delta\mu_k$ and ΔP are presented in the Appendix B.

Our choice for the distance of the Yukawa potential truncation is due to the simplicity reasons, since the other choices for $r_{ij}^{(c)}$ will more substantially increase the number of the moments in the expressions for the chemical potential and pressure (66).

4.2.1. Polydisperse LJ mixture with size polydispersity only

Polydisperse LJ mixture in question was studied using multi-Yukawa pair potential (34) with $N_Y = 8$, $M = 2$ and exponents $\sigma_0 z_n = z_0 k^{(n-1)}$, where $z_0 = 0.896$ and $k = 2.072$. All calculations were carried out with the parent distribution function represented by Schultz distribution (64) with $\gamma = 5$ ($D_\sigma = 0.1(6)$). Similar as in the MC simulation studies [4] distribution function was terminated at $\sigma_c = 3\sigma_0$ and normalized appropriately. As a results LJ potential (63) was fitted by the eight-Yukawa potential (34) for the values of the diameter σ from the interval $0.2\sigma_0 < \sigma < 3\sigma_0$. Yukawa potential coefficients $A^{(nm)}(\sigma)$, which follow from the fitting procedure are collected in the Appendix A. The quality of the fitting procedure can be seen in Figure 6, where we compare original LJ potential and corresponding eight-Yukawa potential for several different values of σ.

In Figure 7 we compare HTA results against MC simulation results [4] for the phase diagram of the LJ model at hand in the (T^*, ρ^*)-plane, where $T^* = k_b T/\epsilon$ and $\rho^* = \rho\sigma_0^3$. For the reference on the same figure we include results of the two methods for the phase diagram of the corresponding monodisperse system. Both MC and HTA predict increase of the critical temperature and slight decrease of the critical density due to polydispersity. For the critical point MC gives $T^*_{\mathrm{cr,MC}} = 1,28$ and $\rho^\star_{\mathrm{cr,MC}} = 0.21$. The corresponding values predicted by the HTA for the critical temperature is about 5% larger ($T^*_{cr,HTA} = 1.344$) and for the critical density is about 8.6% smaller ($\rho^*_{cr,HTA} = 0.192$). For the cloud- and shadow-curve one can see reasonable agreement between HTA and MC results with less accurate agreement for the liquid branch of the shadow curve. In particular both methods predict location of the shadow curve between the two branches of the cloud curve. In accord with MC simulation predictions cloud- and shadow-curve obtained from HTA almost coincide on the temperature-packing fraction plane (T^*, η), where $\eta = \int_0^\infty d\sigma\sigma^3 f(\sigma)$ (Figure 8). Comparison of the theoretical and computer simulation data for the daughter distribution functions of the liquid and gas shadow curves (Figure 9) shows their close agreement. Reasonable agreement was also find for the evolution of the mean size of the particles $\langle\sigma\rangle$ and degree of polydispersity γ along the shadow curve (Figures 10 and 11, respectively). Finally Figure 12 shows position of the critical point on the temperature-packing fraction plane (T^*, η_{cr}) at different values of polydispersity parameter γ. Here HTA reproduces qualitative behavior demonstrated by the MC simulation method with reasonable semi-quantitative agreement between computer simulation and theoretical data. The difference in critical temperature is about 5% and in critical

packing fraction is about 8%.

4.2.2. Polydisperse LJ mixture with size and interaction energy polydispersity

LJ potential (63) with polydispersity in size and interaction energy was fitted by the multi-Yukawa potential (34) with $N_Y = 8$, $M = 2$ and exponents $\sigma_0 z_n = z_0 k^{(n-1)}$ for the values of σ from the interval $0.5\sigma_0 \leq \sigma \leq 3.5\sigma_0$. All calculations were carried out for the parent distribution function represented by Schultz distribution (64) with $\gamma = 50$ ($D_\sigma = 0.0196$). To prevent the appearance of arbitrarily large particles we follow computer simulation studies [12] and terminate the distribution function at $\sigma = \sigma_c$.

In Figure 13 we show the phase diagram for the LJ mixture at hand as obtained from the HTA together with MC results for the cloud curves at two different values of the upper size cutoff $\sigma_c = 1.4\sigma_0$ and $\sigma_c = 1.6\sigma_0$. Both methods predict a substantial shift of the gas branch of the cloud curve into the direction of larger temperatures caused by the different values of σ_c. Quantitative agreement between theoretical and computer simulation methods is less satisfactory with about 9% difference in the critical temperature. Critical density as predicted by HTA almost coincide with the MC critical density. Similarly different values of σ_c affect the distribution functions of the coexisting phases (Figure 14), shifting the liquid shadow phase distribution function into the direction of larger particles. Here quantitative agreement between theory and MC simulation method is not very good. In addition we calculate distribution function of the liquid shadow phase at upper size cut off $\sigma_c = 3\sigma_0$. In agreement with the moment free energy method [12] liquid shadow phase distribution function shows strong fractionation effects with additional maximum appearing at $\sigma = \sigma_c$ (Figure 14).

5. Concluding remarks

In this paper we propose HTA for the polydisperse multi-Yukawa hard-sphere fluid mixture. We show that within HTA the model belongs to the family of the "truncatable free energy models" with its thermodynamical properties defined by the finite number of the generalized moments of the distribution function. This property allows us to map the phase coexistence relations that are particularly complex for polydisperse systems onto a coupled set of highly non-linear equations for the unknown moments of the daughter distribution functions. To validate the accuracy of

the HTA we consider several models of polydisperse fluid and calculate their full phase diagrams, which includes binodals, cloud and shadow curves and distribution functions of the coexisting phases. In particular we apply the theory to investigate the phase behavior of polydisperse one-Yukawa hard-sphere mixture with factorizable Yukawa coefficients and polydisperse LJ mixture with polydispersity in interaction energy parameter and/or in size polidispersity. The former model was studied recently utilizing more advanced MSA approach [7] and the latter model was studied using MC simulation method [4,12]. Results of the HTA appear to be in reasonable agreement with corresponding results of the MSA and MC. The accuracy of the HTA predictions ranges from the semi-quantitative in the case of the phase diagram calculations, to quantitative in the case of the distribution function calculations. Although the HTA approach proposed here is less accurate than MSA theory, it is simpler and more flexible. This can make it to be a useful theoretical method in the analysis of the phase behavior of different polydisperse systems.

6. Acknowledgement

We are grateful to N.B.Wilding for providing us with Monte Carlo simulation results presented in this work.

A. Fitting of the Lennard-Jones potential

LJ potential (63) was fitted by the 8-Yukawa potential (34) using the least square method to optimize the Yukawa coefficients $A^{(nm)}(\sigma)$. The function

$$F\left(\left\{A^{(nm)}(\sigma_i)\right\}\right) = \sum_{ij}^{N_\sigma}\sum_{k}^{N_r}\left[V_{LJ}(r_k,\sigma_{1,i},\sigma_{2,j}) - V(r_k,\sigma_{1,i},\sigma_{2,j})\right]^2, \tag{67}$$

was minimized on a 3-dimensional regular grid formed by the variables σ_1, σ_2, r in the intervals $\sigma_{min} \leq \sigma_1, \sigma_2 \leq \sigma_{max}$ and $\sigma_{12,ij} \leq r \leq 3.5\sigma_{12,ij}$ with the number of points $N_\sigma = 20$ and $N_r = 40$. Here $\sigma_{min} = 0.2\sigma_0$ and $\sigma_{max} = 3\sigma_0$ in the case of LJ potential with size polydispersity only and $\sigma_{min} = 0.5\sigma_0$ and $\sigma_{max} = 3.5\sigma_0$ in the case of the LJ potential with size and energy polydispersity.

B. Correction of the expressions for the chemical potential and pressure due to the Yukawa potential truncation

Substituting the integral in the expression for Helmholtz free energy (36) by its truncated counterpart (65) and using the standard relation between Helmholtz free energy, chemical potentials and pressure, we have

$$\Delta\mu_i^{(tr)} = 4\pi\epsilon_0 \sum_n \sum_m \frac{(-1)^m}{z_n} A_i^{(nm)} e^{-z_n\sigma_i} \left[\left(\widetilde{m}_0^{(nm)} - \frac{m_0^{(nm)}}{{z_n}^2} + \frac{m_1^{(nm)}}{z_n} \right) \left(1 + \frac{3z_n\sigma_i}{2} \right) + \frac{3z_n}{2} \left(\widetilde{m}_1^{(nm)} - \frac{m_1^{(nm)}}{{z_n}^2} + \frac{m_2^{(nm)}}{z_n} \right) \right] \quad (68)$$

$$\Delta P^{(tr)} = -2\pi\epsilon_0 \sum_n \sum_m \frac{(-1)^m}{z_n} \left[\left(\widetilde{m}_0^{(nm)} - \frac{m_0^{(nm)}}{{z_n}^2} + \frac{m_1^{(nm)}}{z_n} \right)^2 + 3z_n \left(\widetilde{m}_1^{(nm)} - \frac{m_1^{(nm)}}{{z_n}^2} + \frac{m_2^{(nm)}}{z_n} \right) \left(\widetilde{m}_0^{(nm)} - \frac{m_0^{(nm)}}{{z_n}^2} + \frac{m_1^{(nm)}}{z_n} \right) \right], \quad (69)$$

where $2MN_Y$ new generalized moments $\widetilde{m}_l^{(nm)}$ have been introduced:

$$\widetilde{m}_l^{(nm)} = \sum_k \rho_k \widetilde{m}_l^{((nm))}(k), \quad (70)$$

$$\widetilde{m}_l^{(nm)}(k) = \rho_k \sigma_k^l \varphi\left(z_n, \sigma_k\right) A_k^{(nm)}, \quad l = 0, 1$$

and other MN_Y additional $m_2^{(nm)}$ moments defined in (58) appeared.

References

1. L. Bellier-Castella, H. Xu, and M. Baus, J. Chem. Phys. **113**, 8337 (2000).
2. P. Sollich, J. Phys. (Condens. Matt.) **14**, R79 (2002).
3. H. Xu, L. Bellier-Castello, and M. Baus, *J. Phys: Cond. Matt.* **14**, 12141(2002).
4. N. B. Wilding, M. Fazolo, and P. Sollich, *J. Chem. Phys.* **121**, 6887(2004).
5. M. Fazolo, P. Sollich, and A. Speranza, *React. Funct. Polym.* **58**, 187(2004).
6. J. J. Salacuse, and G. Stell, *J. Chem. Phys.* **77**, 3714(1982).

7. Yu. V. Kalyuzhnyi, and G. Kahl, *J. Chem. Phys.* **119**, 7335(2003); **122**, 1168(2004).
8. Yu. V. Kalyuzhnyi, G. Kahl, and P. T. Cummings, *J. Chem. Phys.* **120**, 10133(2004).
9. Yu. V. Kalyuzhnyi, G. Kahl, and P. T. Cummings, *Europhys. Lett.* **72**, ??(2005).
10. Yu. V. Kalyuzhnyi, G. Kahl, and P. T. Cummings, *J. Chem. Phys.* **123**, 124501(2005).
11. R. Fantoni, D. Gazzillo, and A. Giacometti, *J. Chem. Phys.* **122**, 034901(2005).
12. N. B. Wilding, P. Sollich, and M. Fasolo, *Phys. Rev. Lett.* **95**, 155701(2005).
13. J.-P. Hansen and I.R. McDonald, *Theory of Simple Liquids*, (Academic, New York, 1986) 2nd edition; C. Caccamo, Phys. Rep. **274**, 1 (1996).
14. J.A. Gualteri, J.M. Kincaid, and G. Morrison, J. Chem. Phys. **77**, 52 (1982).
15. Yu.V. Kalyuzhnyi, and G. Kahl, J. Chem. Phys. **119**, 7335(2003).
16. E.N. Rudisill, and P.T. Cummings, Mol. Phys. **68**, 629(1980).
17. Yu.V. Kalyuzhnyi, and P.T. Cummings, Mol. Phys. **87**, 1459(1996).
18. J.J. Salacuse, and G. Stell, J. Chem. Phys. **77**, 3714(1982).
19. N.N. Bogoliubov
20. J.L. Lebowitz, Phys. Rev. A **133**, 895(1964).
21. L. Blum, and J. Høye, J. Phys. Chem. **81**, 1311(1977).
22. G.A. Mansoori, N.F. Carnahan, K.E. Starling, and T.W. Leland, J. Chem. Phys. **54**, 1523 (1971).
23. M. Abramowitz and I.A. Stegun, *Handbook of Mathematical Functions*, Applied Mathematical Series, **55** (Washington: National Bureau of Standards) (1964).
24. G. V. Schultz, *Z. Phys. Chem. Abt. B* **43**, 25(1939)

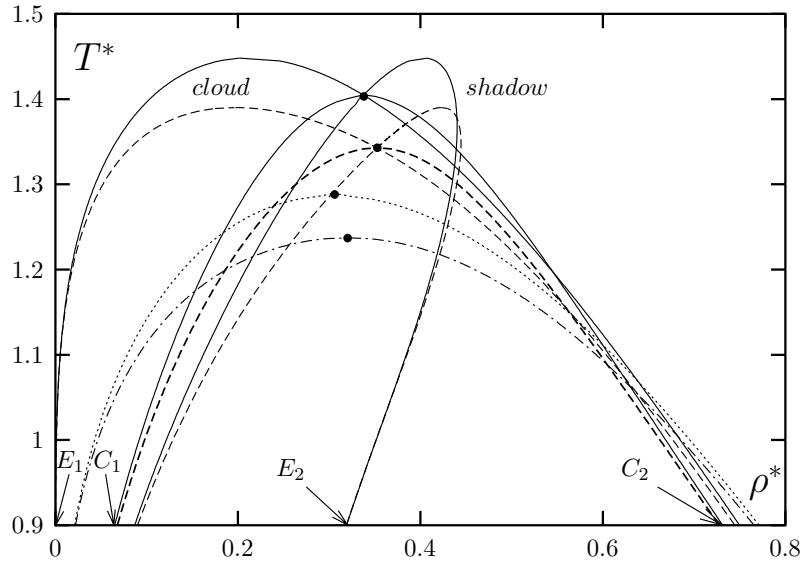

Figure 1.
Phase diagram of polydisperse one-Yukawa hard-sphere mixture, including cloud and shadow curves (as labeled) and critical binodals. HTA results are represented by the solid lines and MSA results by the dashed lines. Two pairs of points are marked on the curves: the points E_1 and E_2 are localized on the cloud curve and shadow curves, respectively, and the points C_1 and C_2 are localized on the gas branch and liquid branch of the critical binodals, respectively. For the reference we include the phase diagram of corresponding monodisperse one-Yukawa model with dotted line representing results of the HTA and dashed-dotted line representing results of the MSA. Filled circle on the top of each binodal denote the position of the critical points.

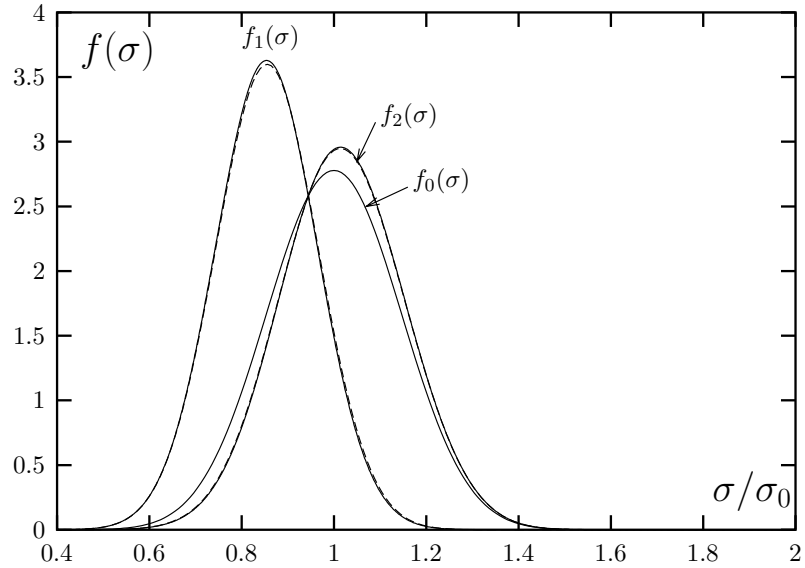

Figure 2.
Parent $[f_0(\sigma)]$ and daughter $[f_1(\sigma)$ and $f_2(\sigma)]$ distribution functions for polydisperse one-Yukawa hard-sphere mixture investigated for the points C_1 and C_2. HTA results are represented by the solid line and MSA results by the dashed line.

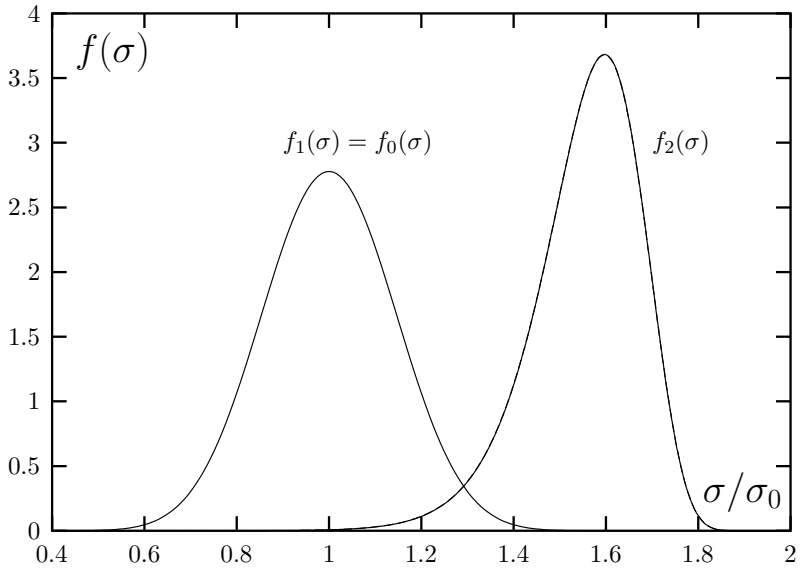

Figure 3.
As in Figure 2 for the points E_1 and E_2.

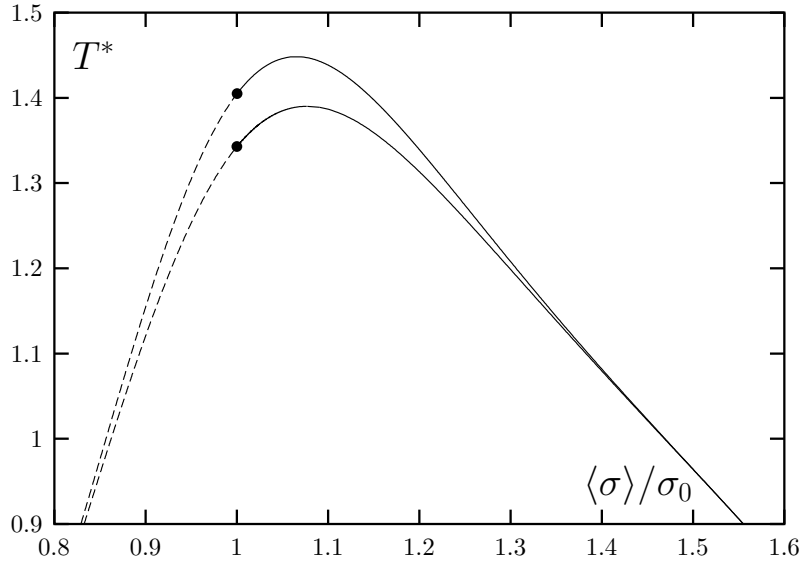

Figure 4.
$\langle\sigma\rangle_i,\ i = 1, 2$ as defined in Eq. (62) along the shadow curve for the polydisperse one-Yukawa mixture. Dashed lines – gas phase ($i = 1$), solid line – liquid phase ($i = 2$). The upper curve represents HTA results and the lower curve – MSA results. Filled circles denote the position of the critical points.

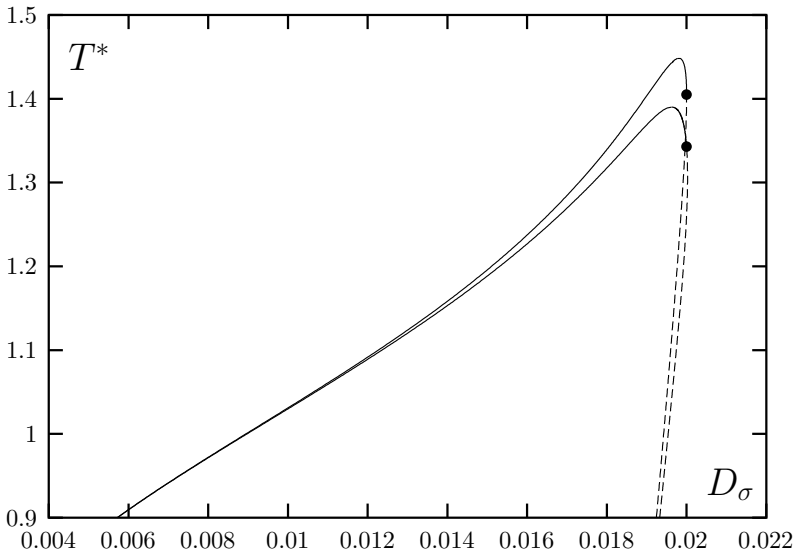

Figure 5.
As in Figure 4 for $D_{\sigma;i},\ i = 1, 2$.

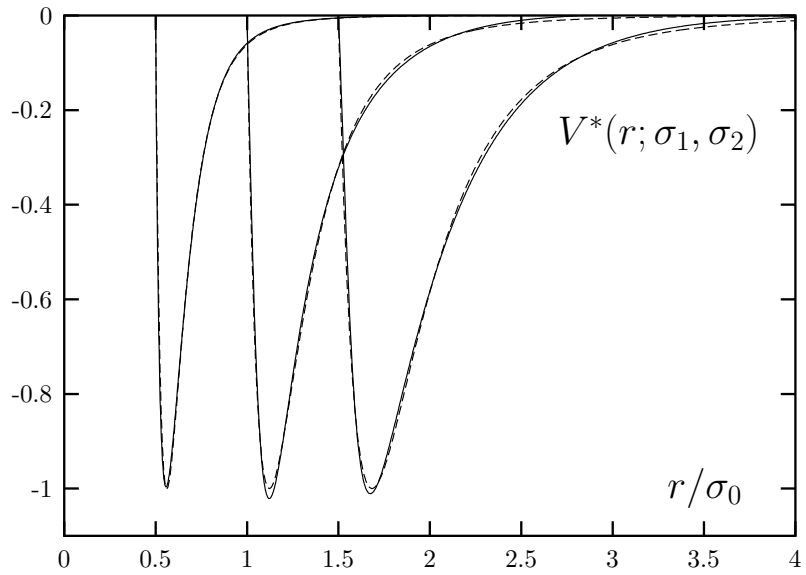

Figure 6.
LJ potential (63) for the model with size polydispersity only (dashed lines) and its 8-Yukawa fit (solid lines) for $\sigma_1 = \sigma_2 = 0.5\sigma_0,\ \sigma_0,\ 1.5\sigma_0$. Both potentials are scaled by the value of the LJ interaction parameter ϵ_0.

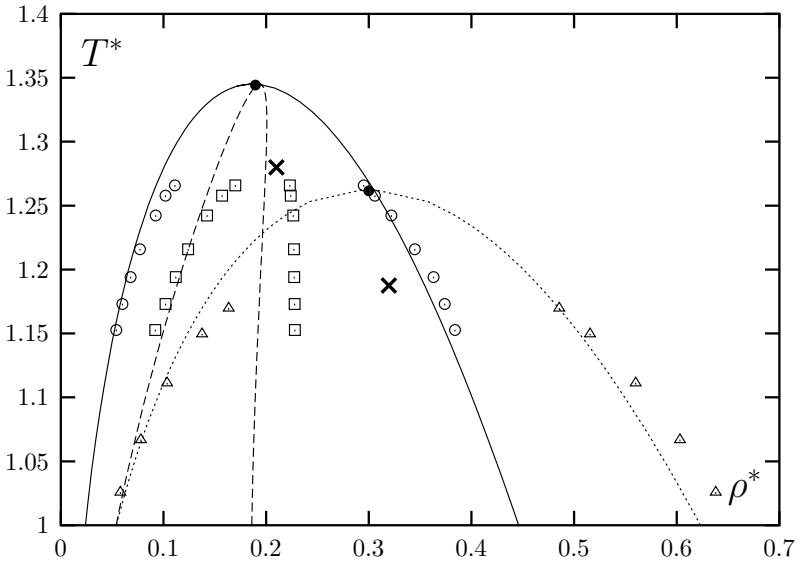

Figure 7.
Phase diagram of polydisperse LJ mixture with size polydispersity only. Lines represent predictions of the HTA and symbols represent predictions of the MC simulation method [4]. Cloud curve is denoted by empty circles and solid line, shadow curve is denoted by empty rectangular and dashed line. For the reference the phase diagram of monodisperse version of the model (empty triangulares and dotted line) is included. Filled circles and crosses show position of the corresponding critical points.

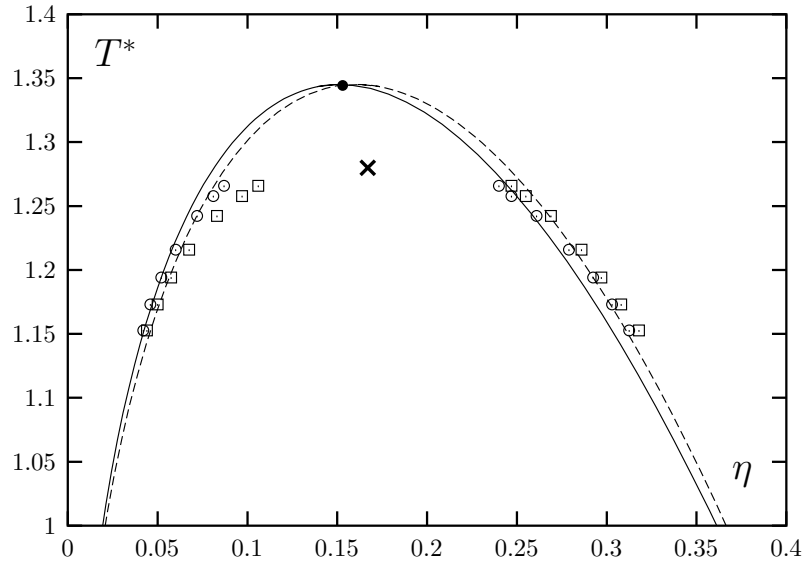

Figure 8.
As in Figure 7 in temperature T^* vs packing fraction $\eta = \pi m_3/6$ coordinates.

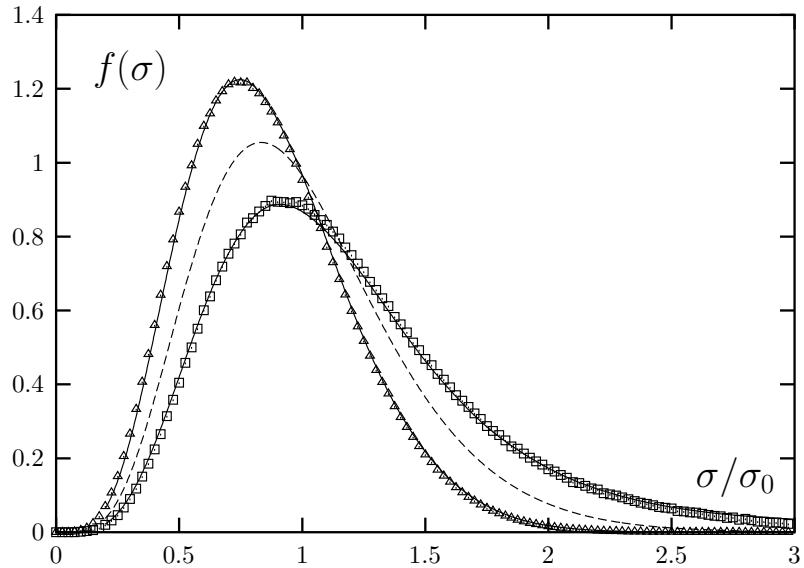

Figure 9.
Distribution function of the shadow gas phase (empty triangles and solid line) and shadow liquid phase (empty rectangular and solid line) at $T^* = 0.91T^*_{cr}$ for polydisperse LJ mixture with size polydispersity only. Lines represent results of the HTA and symbols represent MC simulation results [4]. Dashed line denote distribution function of the parent phase.

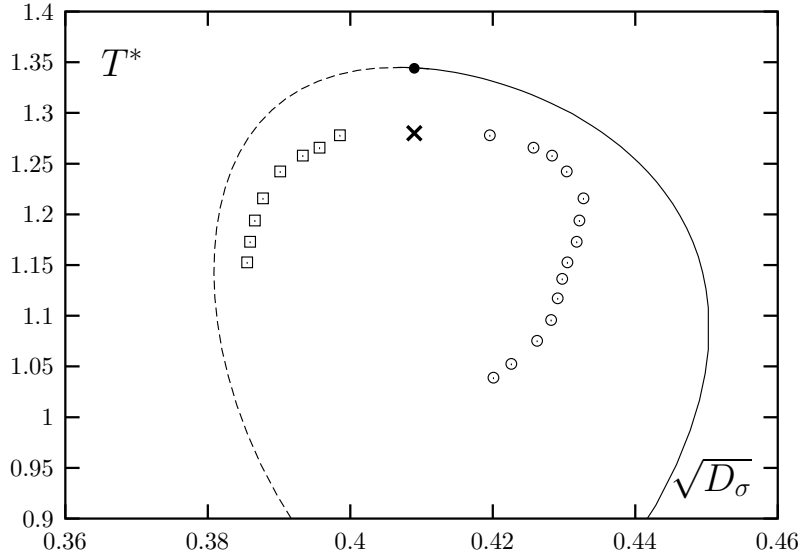

Figure 10.
$\sqrt{D_{\sigma;i}}$, $i = 1, 2$ with $D_{\sigma;i}$ as defined in Eq. (62) along the shadow curve for polydisperse LJ mixture with size polydispersity only. Results of the HTA are represented by the lines and results of the MC simulation method [4] by the symbols. Dashed line and empty rectangular denote the gas phase ($i = 1$), solid line and empty circles denote the liquid phase ($i = 2$). Filled circle and cross show position of the critical point.

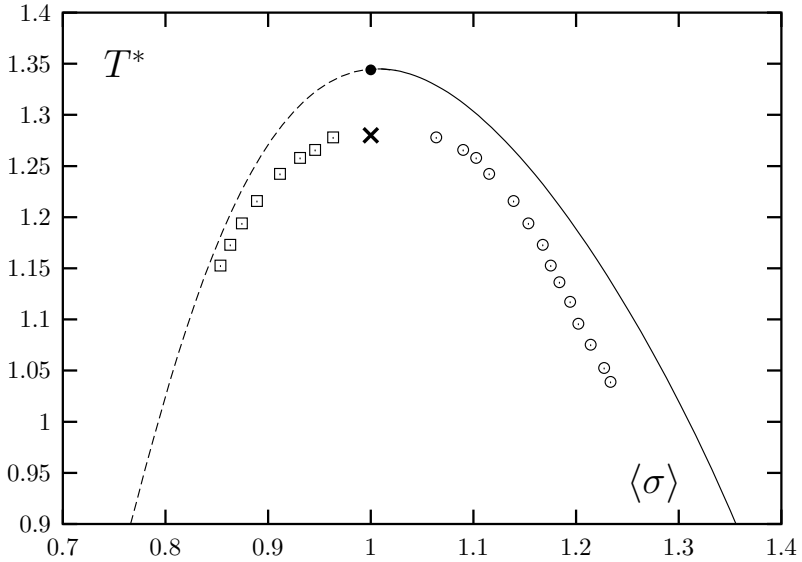

Figure 11.
$\langle\sigma\rangle_i,\ i = 1, 2$ as defined in Eq. (62) along the shadow curve for polydisperse LJ mixture with size polydispersity only. Results of the HTA are represented by the lines and results of the MC simulation method [4] by the symbols. Dashed line and empty rectangular denote the gas phase ($i = 1$), solid line and empty circles denote the liquid phase ($i = 2$). Filled circle and cross show position of the critical point.

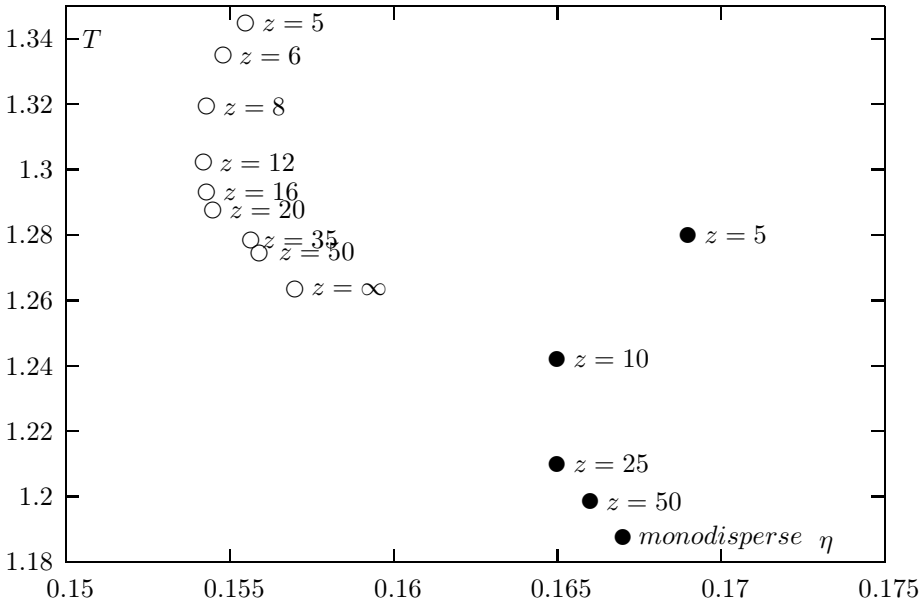

Figure 12.
Position of the critical point on T^* vs η plane. Filled circles denote MC simulation results [4] and empty circles denote results of the present theory.

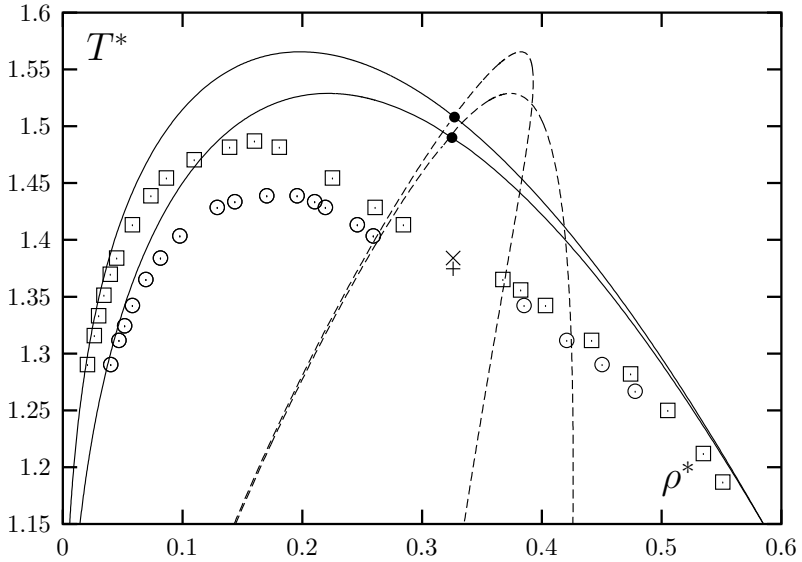

Figure 13.
Phase diagram of polydisperse LJ mixture with size and energy parameter polydispersity. Lines represent predictions of the HTA and symbols represent predictions of the MC simulation method [12]. Cloud curve at $\sigma_c = 1.4\sigma_0$ is denoted by empty circles and lower solid line, cloud curve at $\sigma_c = 1.6\sigma_0$ is denoted by empty rectangularand higher solid line. Shadow curves are denoted by the dashed lines.

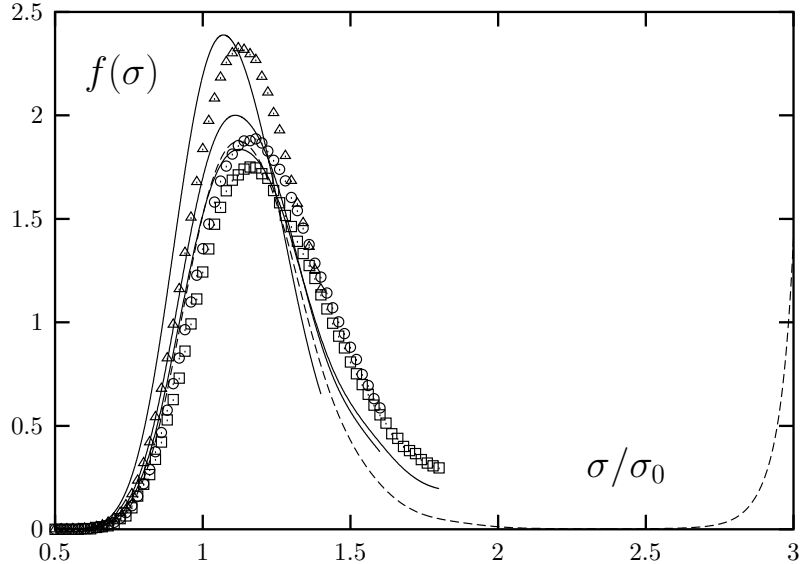

Figure 14.
Distribution functions of the shadow liquid phase at $T^* = T_{cr,MC}$ as predicted by MC simulation method [12] (symbols) and at $T^* = T_{cr.HTA}$ as predicted by HTA (solid lines). $\sigma_c = 1.4\sigma_0$ (empty triangles and solid line), $\sigma_c = 1.6\sigma_0$ (empty circles and solid line) and $\sigma_c = 1.8\sigma_0$ (empty rectangular and solid line) from the top to the bottom at $\sigma = \sigma_0$ and $\sigma_c =$. Dashed line represents results of the HTA at $\sigma_c = 3\sigma_0$.